Available online at www.sciencedirect.com

ScienceDirect

Advances in Space Research 73 (2024) 3486–3493

ADVANCES IN SPACE RESEARCH
(a COSPAR publication)

www.elsevier.com/locate/asr

Equatorial plasma bubble association with lower atmospheric gravity waves – Further evidences

R.N. Ghodpage [a,*], A. Taori [b], M.K. Patil [c], O.B. Gurav [d], R.P. Patil [e], S. Sripathi [f]

[a] M. F. Radar, Indian Institute of Geomagnetism, Shivaji University Campus, Kolhapur 416 004, India
[b] Earth & Climate Science Area, National Remote Sensing Centre, Hyderabad 500 037, India
[c] School of Physical Sciences, Swami Ramanand Teerth Marathwada University, Nanded 431 606, India
[d] Department of Physics, Bharati Vidyapeeth (Deemed to Be University), Yashwant Rao Mohite College of Arts, Science and Commerce, Pune 411 030, India
[e] Indian Institute of Tropical Meteorology, Pune 411 008, India
[f] Indian Institute of Geomagnetism, Navi Mumbai 418 210, India

Received 2 December 2022; received in revised form 25 May 2023; accepted 31 May 2023
Available online 7 June 2023

Abstract

Space based radio wave communication and navigation has become need of the society. Atmospheric (thermospheric-ionospheric) processes, such as Equatorial Plasma Bubbles (EPBs), affect the radio waves propagating through this region, causing heavy perturbations on signals received at ground. This paper investigates the causative mechanism of EPB through the ground based remotely sensed imaging observations of O (^{1}S) 557.7 nm and O (^{1}D) 630.0 nm emissions emanating from the upper mesosphere (~100 km altitudes) and thermosphere-ionosphere (~250 km altitudes) over a low-latitude station, Kolhapur (16.8° N, 74.2° E, and dip lat. 10.6°N). Our investigation revealed that the gravity waves evident in OI557.7 nm images exhibit a close association with the observed EPB structures. These mesospheric gravity waves were found to travel from the South to North with horizontal wavelengths ~35 and ~56 km on 13–14 April and 26–27 April 2015, respectively. The thermosphere-ionosphere measurements exhibited occurrence of the North–South aligned EPB moving to the east with an inter depletion distance (IDD) equal to ~44 km and ~64 km. These results provide evidences on association of the gravity waves with the EPB.

Keywords: Gravity wave; EPB; IDD

1. Introduction

In a well-connected society, the earth's ionized medium, viz., the ionosphere, plays a major role in the satellite based communication and navigation systems. This ionized medium is a subset of the earth's upper atmosphere, which encompasses the thermosphere-ionosphere system and exhibits myriad phenomena that occur due to the neutral-ion interaction under the influence of earth's electric and magnetic fields (e.g., Hargreaves, 1992). Due to the ability of the ionosphere to refract the high frequency radio waves, large changes in the ionospheric densities can disrupt the propagation of radio waves and, hence, may result in the communication and navigation blackouts. Due to increasing dependence of the society on the satellite based communication and navigation, there is a need to monitor and understand the ionosphere processes relentlessly by remote sensing of the phenomena either by the geo-stationary satellites or ground-based instruments.

Spread-F in the bottomside evolves to topside plasma bubbles is one of the conspicuous phenomena, which occur in the nighttime ionosphere (Booker and Wells, 1938). Generally, EPBs are observed within the equatorial and

* Corresponding author.
E-mail address: rupesh.g@iigm.res.in (R.N. Ghodpage).

https://doi.org/10.1016/j.asr.2023.05.056
0273-1177/

low-latitude regions of narrow band of ±20°dip latitude after the sunset. The Rayleigh-Taylor (RT) instability is believed to be the process behind the occurrence of ESF (e.g., Kelley et al., 1981, Dungey, 1956, Balsley et al., 1972). Some of the investigations (e.g., Kudeki et al., 2007) hypothesized the during the sunset times, the equatorial ionosphere exhibits a strong shear flow with eastward winds at the F-region peak and westward winds near the base height, which can persist for a few hours (e.g., Hysell et al., 2005) to provide suitable seed perturbation for the growth of the RT instability. Tsunoda et al. (2010) have shown the presence of large scale wave structures prior to the onset of the ESF occurrences, though sources of these structures remain debatable. A novel study by Kelley et al. (1981) after that Prakash and Pandey (1985) suggested that electric fields can be generated by the gravity wave winds. This was followed by a proposal by Hysell et al. (1990) that gravity waves may interact with small scale Rayleigh-Taylor modes which enabled a strong foundation about gravity wave seeding the EPBs occurrences. Fagundes et al. (1995) suggests that thermospheric winds have only a minor role in the production of equatorial ionospheric plasma depletions. An examination of the nocturnal intensity variations of simultaneous mesospheric (E-region) emissions (OI557.7 nm, O_2 atm. 864.5 nm, NaD 589.0 nm, and OH (9–4) 775.0 nm) on observed nights studied reveals the presence of gravity waves, indicating a possible link between wave processes in the mesosphere and F-region irregularities. This theory was further strengthened by several events during spread FEx campaign (e.g., Fritts et al., 2008). Paulino et al., 2011 observed medium-scale gravity waves in OH airglow images were recorded during the Conjugate Point Experiment (COPEX) program at Boa Vista (2.80°N, 60.7 °W, dip angle 21.73°N) during October to December 2002. The majority of the waves propagate northwest, indicating that they originate southeast of Boa Vista. They had observed simultaneous plasma bubble activity in the OI 630 nm images. The distances between bubble depletions show a linear relationship with the wavelengths of the gravity waves seen in the mesosphere, indicating that the mesospheric medium scale gravity waves were directly seeding the equatorial plasma bubbles. Using airglow emission monitoring and very high frequency (VHF) radar measurements, Patra et al. (2013) showed gravity wave like structures just before the EPB occurrences. Further evidences on the role of gravity waves in EPB occurrences and structuring were provided by several investigators (e.g., Makela et al., 2010, Sivakandan et al., 2019, Takahashi et al., 2009). Takahashi et al. (2009) provided direct evidence of plasma bubble formation and mesospheric gravity wave activity in the mesosphere. They used airglow all-sky imagers to measure equatorial plasma bubbles and mesospheric gravity waves simultaneously using OI 630.0 nm and OHNIR emissions. They found a good correlation between gravity wave horizontal wavelength in the mesosphere with the inter depletion distance of the plasma bubble. In addition to optical techniques, they have also utilized Digisonde and VHF coherent radar to study the ionospheric density and density fluctuations. They suggested that mesospheric gravity waves can reach the ionosphere to provide seed perturbation for the RT instability.

Taori et al. (2010) presented simultaneous monitoring of mesospheric and thermospheric airglow emissions over low latitudes in the Pacific sector to study the optical signature of mesospheric waves during equatorial plasma bubbles (EPBs). Two case studies show two consecutive nights, one with EPBs and one without. They showed that short-period gravity waves with periods less than 3 h had larger wave growth between the OH and O_2 emission altitudes during EPB nights. In another study of co-located observations from Gadanki (13.5°N, 79.2°E), an all-sky airglow imager, Gadanki Ionospheric Radar Interferometer (GIRI), and Tirunelveli Ionosonde observations to investigate the role of gravity waves in the generation of equatorial plasma bubbles (EPBs) during geomagnetic quiet conditions by Sivakandan et al. (2019). It was noted that despite the all four nights' ionospheric peak altitudes (h′F) values are greater than 350 km, only three of the nights exhibit EPBs in the OI 630 nm airglow emission and radar plumes. It was observed that at the OH peak emission altitudes and E-region, three nights exhibited periodic oscillations which were argued to be the gravity wave signatures.

Recently, using "Global-scale Observations of Limb and Disk" (GOLD) mission of National Aeronautics and Space Administration, Aa et al. (2020) presented coordinated space borne and ground based data and found presence of wavelike structures at the bottom-side ionosphere which were argued to be signatures of atmospheric gravity waves.

The present report originality is enhanced by the fact that all of the measurements were taken in the same month (April 2015) and season, when the geomagnetic field was relatively calm and there were no full moons. Prior research may have made use of different conditions, such as a different wavelength (OI630.0 nm), or OH of emission. We used emission images of OI 630.0 nm (altitude of ~250 km) and OI557.7 nm (corresponding to an altitude of ~97 km). Therefore, we include the phrase "further evidence" in the title of our work.

In the present study, we use airglow data from Kolhapur (16.8°N, 74.2°E, dip lat. 10.6°N) and ionosonde data from Tirunelveli (8.73°N, 77.7°E, dip lat.1.6°N) to investigate further evidences to support the role of gravity waves in the observed EPB characteristics. For a fair study, we selected similar month so that background processes at mesospheric altitudes and ionospheric conditions do not vary significantly. Further, to eliminate the impact of disturbance dynamo and any prompt penetration (e.g., Klimenko and Klimenko, 2012) we selected 13–14 and 26–27 April 2015 when Ap values were 6 and 8, respectively.

2. Measurement method:

In this work we use two instrument data namely, *All-Sky Imager* (ASI) at Kolhapur and ionosonde at Tirunelveli.

2.1. All-Sky imager

The **All-sky** imager (ASI) operating over Kolhapur (16.8° N, 74.2° E, and 10.6° N dip lat.) monitors OH, O (^{1}S) 557.7 nm and O (^{1}D) 630.0 nm night airglow emissions with the help of temperature controlled interference filters (transmission 50–90%). The front-end optics collects the incoming radiation in 180° field of view (FOV) with a fisheye lens (f/4 Mamiya RB67). The integration times used for the above stated emissions in the present setup are 120 s, 120 s, 30 s respectively. The movement of filter wheel is synchronized with charge coupled device (CCD) detector operation. The CCD camera uses a back illuminated 1024 × 1024 pixel CCD (Pixis, ~1 mega pixel resolution) of 24 μm size, 100% fill factor and 16 bit depth. To enhance the signal-to-noise ratio of the present set-up we bin the images for 2 × 2 pixels making an effective 512 × 512 super pixels image on the chip. We restrict the image to FOV of 140° to avoid the nonlinearity arising due to curvature effects and also to minimize surrounding lights at lower elevation angles. Ghodpage et al. (2014) elaborates the ASI details and analysis procedures adopted in the present study.

2.2. Canadian advanced digital ionosonde

We use Canadian Advanced Digital Ionosonde (CADI) data recorded over Tirunelveli (8.73°N, 77.7°E, dip. lat.1.6° N). Its frequency range is between 1 and 20 MHz operated with different temporal resolutions. It consists of a delta type antenna along with the four receivers mounted east–west and magnetic north–south direction, capable of measuring the irregularity drift in the east–west as well as the north–south directions. CADI is operated in frequency sweep mode over Tirunelveli and continuously measures the basic ionospheric parameters. Detailed information of the system is available in the literature (e.g., Sripathi et al., 2016).

3. Results

Sample O (^{1}D) 630.0 nm night airglow images depicting the EPB occurrences on both the nights (13–14 April 2015 and 26–27 April 2015) are shown in Fig. 1. The dark regions in the images depicting the regions of decreased intensity, i.e., the plasma bubbles are noteworthy**,** on both the nights. These depleted regions of intensity are indicated by the yellow arrow. The ASI images are unwrapped onto equidistant grid with FOV 100°. The standard method has been utilized for unwrapping (Narayanan et al., 2009).

To emphasize the recurring EPBs on these nights, the time variation of O(^{1}D) 630 nm emissions, centered on zenith with 5 × 5 pixel area are plotted in Figs. 2a and 2b. We note that 13–14 April data was dominated by the multiple bite outs exhibiting recurring EPB features, while, the intensity plots for 26–27 April are characterized with two large bite outs with small EPB structures as shown in Fig. 2b. This intensity plot shows that on 13–14 April 2015, the depleted regions passed by the Kolhapur at around 1420 UT, 1515 UT 1600 UT, 1650 UT, 18 UT, 19 UT, 20 UT, 2030 UT and 2110 UT. A careful inspection of the plot **2(b)** reveal that after a small depleted structure at 1520 UT, a big depleted region was noted, reaching the minimum intensity around 1800 UT, followed by another depleted structure at 20 UT, 21UT, 2220 UT and 23 UT. Further, the depleted regions with small intensity decrease during 21–23 UT occurred within a larger depleted regions passing by the Kolhapur during 21–23 UT with its overhead presence at 2230 UT.

As the ionospheric conditioning such as pre-reversal enhancement (Rishbeth, 1971a, 1971b, Heelis et al., 1974, Farley et al., 1986, Haerendel and Eccles, 1992; Kelley, 1989) makes the background conducive for the occurrence of EPBs, it is prudent to look for the variation in the basic ionospheric parameters (base height and peak frequency of the ionosphere) which are monitored by the ionosonde over the equatorial station. The base height (h'F) and peak frequency (foF2) of the F-layer on both nights are shown in Fig. 3. Horizontal gray bar in both plots depict the occurrence time of EPBs. We note that h'F values went beyond 350 km before the occurrences of EPBs on both the nights. The foF2 values show significant variability with perturbation amplitudes more than 20%, indicating large changes in the electron densities.

To understand the spatio-temporal variability of EPB, keogram analysis has been carried out. In a keogram analysis a strip centered on the zenith with width of 10x10 is clipped in the East-West direction and stacked in time domain to showcase the spatial structures of EPB along-with its time variation. Fig. 4 depicts the keograms produced for OI 630 nm on both nights. We observe that various places of decreasing intensity may be seen on April 13–14, supporting the findings in Fig. 4. On 26–27 April a bright streak visible in the west direction of the keogram is due to the moon transit. Depleted intensity regions are also visible between 1900 and 2100 UT and weak EPB structure occurring at 2220 and 2300 UT.

4. Discussion

It is evident from Figs. 1–4 that the EPB signatures noted on the two nights are significantly different. The EPB structures noted on 26–27 April 2015 are broad compared to the one noted on 13–14 April 2015. We note that background ionosphere was similar on both nights (similar h'F and foF2 values) and influences arising due to the geomagnetic disturbances are absent on both nights (Ap values 6

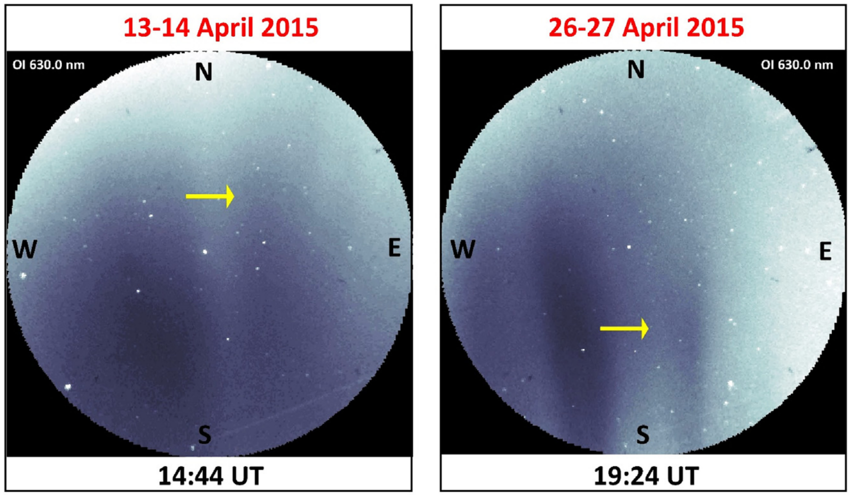

Fig. 1. Images illustrating the depletion (EPB) of North-South aligned structures in OI 630.0 nm airglow data on (a) April 13–14 and (b) April 26–27, 2015.

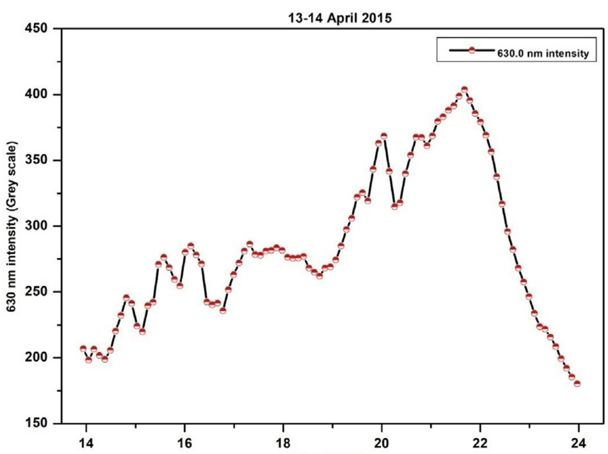

Fig. 2a. Zenith (5 × 5) intensity plot for observations corresponding to 13–14 April 2015, displaying depletion event occurrences.

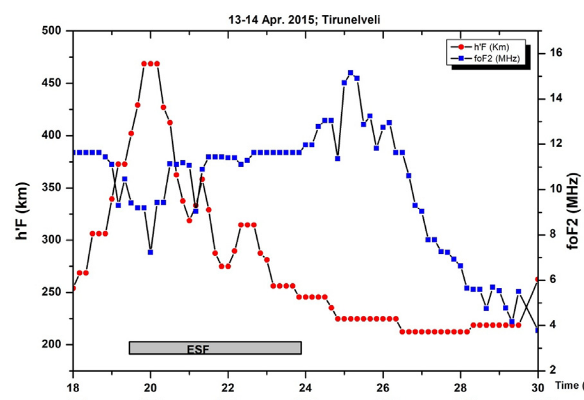

Fig. 3a. Ionosonde data corresponding to the 13–14 April 2015. Horizontal grey bar shows ESF occurrence time noted in the ionosonde data.

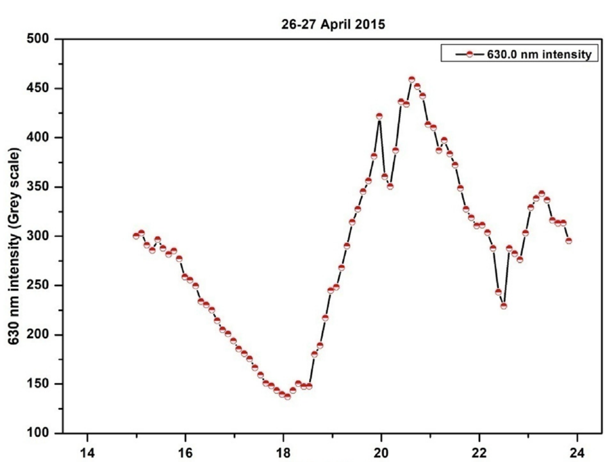

Fig. 2b. Same as Fig. 2a but for 26–27 April 2015.

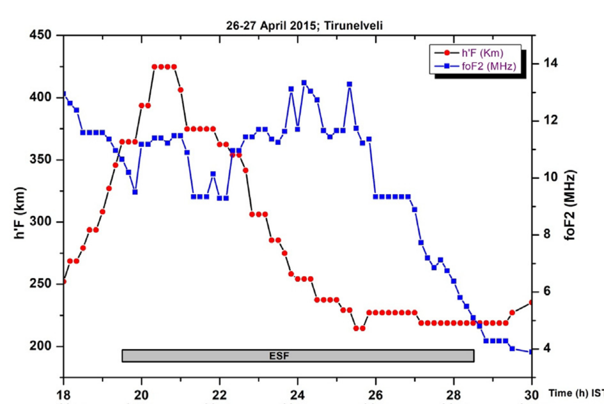

Fig. 3b. Same as Fig. 3a but for 26–27 April 2015.

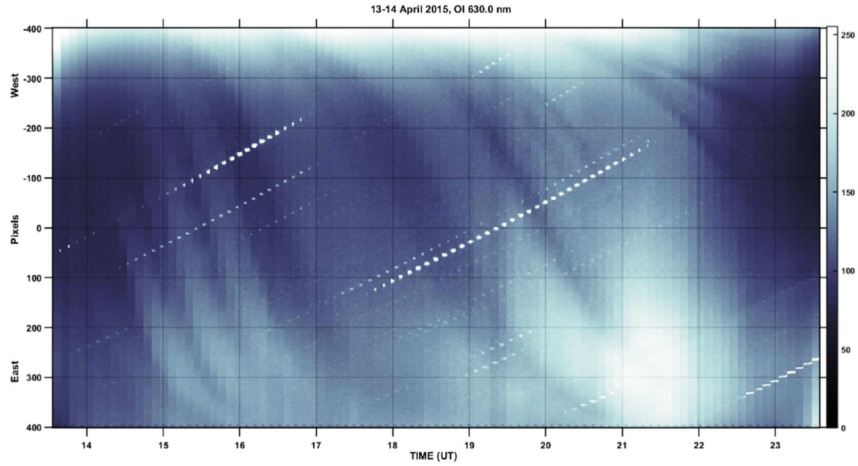

Fig. 4a. On the 13–14 April 2015, a series of 630 nm images highlighted the occurrence, progression, and propagation of depletions. The dark bands indicate where the depletion structures are located.

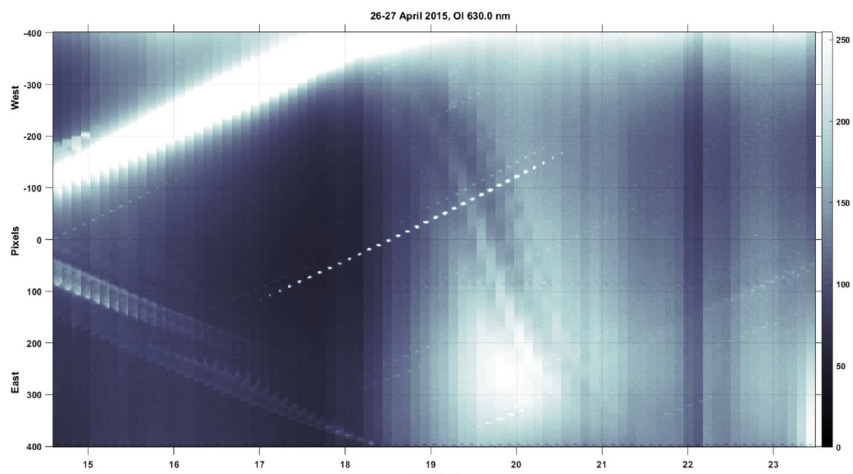

Fig. 4b. Same as Fig. 4a but for 26–27 April 2015.

and 8). Both cases occurred during geomagnetic quiet conditions, and the large scale wave structures were absent on both days. As a result, the most plausible explanation for the observed differences could be seed perturbation of lower atmospheric origin. It is also noted that some of the gravity waves may be able to penetrate the middle atmosphere and reach the thermosphere (e.g., Vadas, 2007). Thus, gravity waves are the remaining perturbation as far as the seeding the EPB is concerned. Taori et al. (2012) reported that gravity wave amplitudes and periods have a role in the observed plasma plume structures in the VHF radar backscatter echoes. Further, Makela et al. (2010) reported close resemblances between the periodic spacing of EPBs and horizontal wavelengths of mesospheric gravity waves.

We estimate the gravity wave characteristics observed on this night based on the O (^{1}S) images. Fig. 5 plots the wave features noted on 13–14 April and 26–27 April 2015. It is noteworthy that on these nights, the oscillatory features were propagating towards north at angles of,

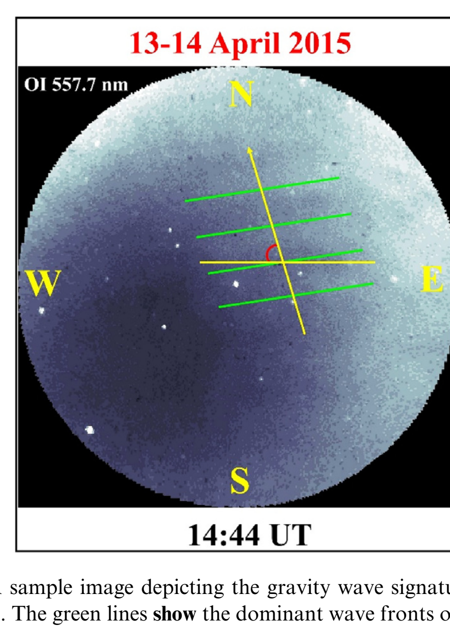

Fig. 5a. A sample image depicting the gravity wave signatures on 13–14 April 2015. The green lines **show** the dominant wave fronts observed while the yellow arrows reveal their propagation direction at an angle θ.

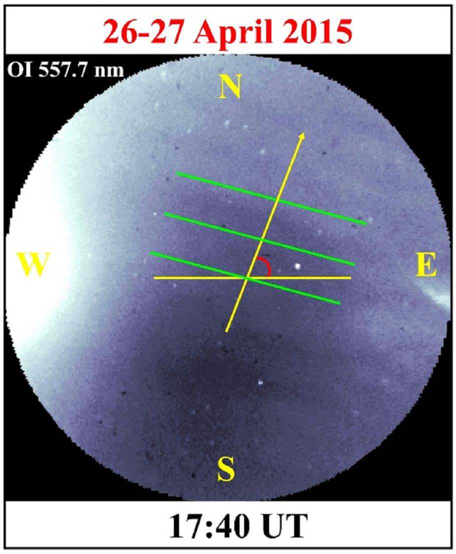

Fig. 5b. Same as Fig. 5a but for 26–27 April 2015.

approximately, 354° and 28°, and velocities of 36 ms^{-1} and 48 ms^{-1}, on 13–14 April and 26–27 April 2015, respectively.

The horizontal wavelengths of the observed gravity waves are estimated to be 36 ± 4 km on 13–14 April 2015 and 56 ± 6 km on 26–27 April 2015. The observed amplitudes of these waves are noted to be 2.3% and 3.9%, respectively, on 13–14 and 26–27 April 2015, which are significant as reported by Sivakandan et al. (2019). Varney et al. (2009) suggested that slightly inclined gravity wave propagation produces meaningful vertical drifts and, hence, polarized electric fields, which in turn acted as seeding for the RT instability. They also noted that small amplitudes were best suited for seeding the Rayleigh-Taylor instability. It meant that when it comes to the structuring of the plumes, the small amplitudes are best detected. Further, report by Taori et al. (2011) noted occurrence of similar wave periodicity in the middle atmospheric temperature and E region drift data and the estimated vertical wavelength of the middle atmospheric waves. These aspects clearly indicated that the variations observed in the E region field aligned irregularities (FAI) drifts are due to the variations in the electric field associated with the dynamo action of these gravity waves (e.g., Prakash and Pandey, 1985).

Under the assumption that similar processes are occurring, in the image data, it would be obvious to see differences in the observed inter depletion distances (IDD) in both the nights. To evaluate this, we calculated the inter depletion distances which are shown in Fig. 6. We noted that the IDD on 13–14 April 2015 was about 44 ± 5 km while that on 26–27 April 2015 was noted to be 64 ± 6 km. This suggests that the depletion structures noted on 26–27 April were broader by about 1.5 times than the one noted on 13–14 April 2015. Another EPB structure also seen in Fig. 6b and its IDD is 32 ± 6 km. After the 100° full field of view of a fish-eye lens, it is typically barrel distortion that makes the scales nonlinear. Therefore, we have restricted ourselves to 120° where we have confidence in the observed features within 100°. Therefore, we avoid features that are extremely distant from the zenith. Table 1 present the parameters noted on these nights with respect to the IDD and wavelength of gravity waves. It is noteworthy that the gravity wave wavelengths on 13–14 April were about 36 km while on 26–27 April were 56 km. This suggests very close resemblance in the gravity wave wavelength and

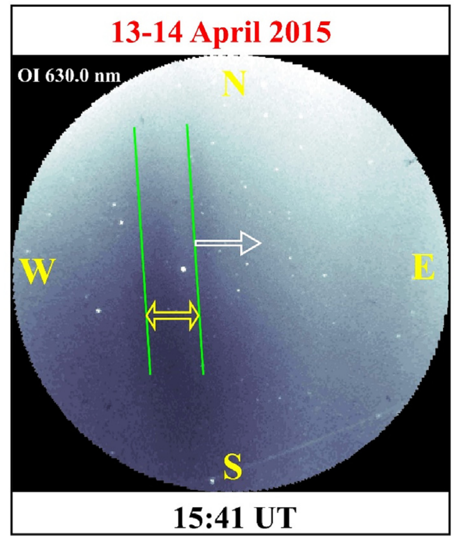

Fig. 6a. A sample OI 630.0 nm image depicting the inter depletion distance (IDD) on 13–14 April 2015. The yellow arrow shows the distance between two depletions while the white arrow shows movement of the depletion.

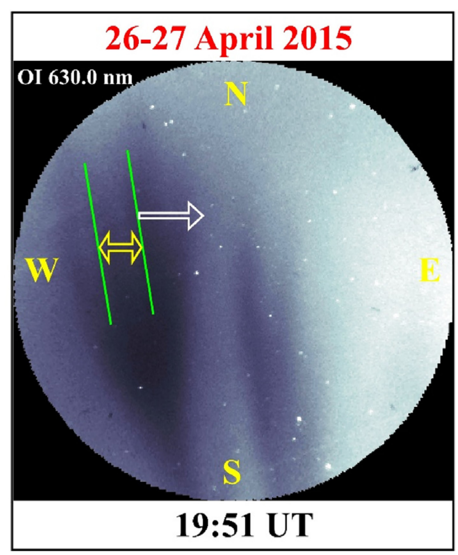

Fig. 6b. Same as Fig. 6a but for 26–27 April 2015.

Table 1
Estimated IDD and horizontal wavelength of gravity waves.

Sr. No	Observation day	Phase velocity (m/s)	Horizontal wavelength (km)	Propagation Angle (θ)	IDD (km)
1	13–14 April 2015	36.31	36.08	354.50	44.72
2	26–27 April 2015	48.46	56.58	28.50	64.75

IDD. As the direct vertical propagation of mesospheric gravity waves from about 100 km to the base height of ionosphere in short timescale is not tenable, we therefore, trust that gravity waves through polarized electric fields may have got mapped. These signatures are therefore reflected a kin onto the IDD noted in the plasma bubbles.

Overall, our data adds on the available evidences supporting the gravity wave seeding hypothesis on the occurrences of EPB structures. We believe that moderate amplitudes of gravity waves while traveling in a proper angle to the magnetic fields can produce the gravity wave electric fields that can map to the F-region and reflect themselves as EPB structures.

5. Conclusions

We report two cases of EPB occurrences out of six observed which were under the quiet geomagnetic conditions when large electron density variations were noted. The gravity waves at upper mesosphere were found to travel in the inclined plane to the geomagnetic field lines with horizontal wavelengths of, approximately, 36 km and 56 km, while the corresponding EPB structures revealed the inter depletion distances to be 44 km and 64 km, respectively. We believe that this signifies a close association and imprints of the mesospheric gravity waves on the EPBs. Further efforts would be to carry out year around the simultaneous mesospheric and thermospheric observations to put more light on the role of GWs on EPB occurrences and its seasonal preferences.

Declaration of Competing Interest

The authors declare that they have no known competing financial interests or personal relationships that could have appeared to influence the work reported in this paper.

Acknowledgements

The nightglow ASI campaign observations are carried out at Shivaji University, Campus Kolhapur, India by Indian Institute of Geomagnetism (IIG), Navi Mumbai. Authors thank Director, IIG, Mumbai and Director, NRSC, ISRO, Hyderabad for encouragements provided for this collaborative investigation. The data presented can be made available upon request to the RG and SS.

Appendix A. Supplementary material

Supplementary material to this article can be found online at https://doi.org/10.1016/j.asr.2023.05.056.

References

Aa, E., Zou, S., Eastes, R., Karan, D.K., Zhang, S.-R., Erickson, P.J., Coster, A.J., 2020. Coordinated ground-based and space-based observations of equatorial plasma bubbles. J. Geophys. Res.: Space Phys. 125. https://doi.org/10.1029/2019JA027569 e2019JA027569.

Balsley, B.B., Haerendel, G., Greenwald, R.A., 1972. Equatorial spread *F*: Recent observations and a new interpretation. J. Geophys. Res. 77 (28), 5625–5628. https://doi.org/10.1029/JA077i028p05625.

Booker, H.G., Wells, H.W., 1938. Scattering of radio waves by the F-region of the ionosphere. Terrest. Magn. Atmos. Electr. 43 (3), 249–256. https://doi.org/10.1029/TE043i003p00249.

Dungey, J.W., 1956. Convective diffusion in the equatorial *F* region. J. Atmos. Terrestr. Phys. 9, 304–310. https://doi.org/10.1016/0021-9169(56)90148-9.

Fagundes, P.R., Sahai, Y., Bittencourt, J.A., Takahashi, H., 1995. Relationship between generation of equatorial F-region plasma bubbles and thermospheric dynamics. Adv. Space Res. 16 (5), 117–120. https://doi.org/10.1016/0273-1177(95)00180-M.

Farley, D.T., Bonelli, E., Fejer, B.G., Larsen, M.F., 1986. The prereversal enhancement of the zonal electric field in the equatorial ionosphere. J. Geophys. Res. 91 (A12), 13723–13728. https://doi.org/10.1029/JA091iA12p13723.

Fritts, D.C., Vadas, S.L., Riggin, D.M., Abdu, M.A., Batista, I.S., Takahashi, H., Medeiros, A., Kamalabadi, F., Liu, H.L., Fejer, B.G., Taylor, M.J., 2008. Gravity wave and tidal influences on equatorial spread F based on observations during the Spread F Experiment (Spread FEx). Ann. Geophys. 26, 3235–3252. https://doi.org/10.5194/angeo-26-3235-2008.

Ghodpage, R.N., Taori, A., Patil, P.T., Gurubaran, S., Sripathi, S., Banola, S., Sharma, A.K., 2014. Simultaneous optical measurements of equatorial plasma bubble (EPB) from Kolhapur (16.81°N, 74.21°E) and Gadanki (13.51°N, 79.21°E). J. Atmosp. Solar-Terrestr. Phys. 121, 196–205.

Haerendel, G., Eccles, J.V., 1992. The role of the equatorial electrojet in the evening ionosphere. J. Geophys. Res. 97 (A2), 1181–1192. https://doi.org/10.1029/91JA02227.

Hargreaves, J.K., 1992. The Solar-terrestrial Environment. Cambridge University Press, London.

Heelis, R.A., Kendall, P.C., Moffett, R.J., Windle, D.W., Rishbeth, H., 1974. Electrical coupling of the *E*- and *F*-regions and its effect on *F*-region drifts and winds. Planet. Space Sci. 22 (5), 743–756. https://doi.org/10.1016/0032-0633(74)90144-5.

Hysell, D.L., Kelley, M.C., Swartz, W.E., Woodman, R.F., 1990. Seeding and layering of equatorial spread F by gravity waves. J. Geophys. Res. 95 (A10), 17253. https://doi.org/10.1029/ja095ia10p17253.

Hysell, D.L., Kudeki, E., Chau, J.L., 2005. Possible ionospheric preconditioning by shear flow leading to equatorial spread F. Ann. Geo-Phys. 23 (7), 2005–2647. https://doi.org/10.5194/angeo-23-2647-2005.

Kelley, M.C., Larsen, M.F., LaHoz, C., McClure, J.P., 1981. Gravity wave initiation of equatorial spread F: A case study. J. Geophys. Res. 86 (A11), 9087–9100. https://doi.org/10.1029/JA086iA11p09087.

Kelley, M.C., 1989. The Earth's ionosphere, plasma physics and electrodynamics, Int. Geophys. Series, Vol. 43, Academic, San Diego, Calif.

Klimenko, M.V., Klimenko, V.V., 2012. Disturbance dynamo, prompt penetration electric field and overshielding in the Earth's ionosphere during geomagnetic storm. J. Atmos. Sol. Terr. Phys. 90–91, 146–155. https://doi.org/10.1016/j.jastp.2012.02.018.

Kudeki, E., Akgiray, A., Milla, M., Chau, J.L., Haysell, n.d., 2007. Equatorial spread F initiation: Post-sunset vortex, thermospheric winds,gravity waves. J. Atmos. Sol. Terr. Phys. 69, 2416–2427. https://doi.org/10.1016/j.jastp.2007.04.012.

Makela, J.J., Vadas, S.L., Muryanto, R., Duly, T., Crowley, G., 2010. Periodic spacing between consecutive equatorial plasma bubbles. Geophys. Res. Lett. 37, L14103. https://doi.org/10.1029/2010GL043968.

Narayanan, V.L., Gurubaran, S., Emperumal, K., 2009. A case study of a mesospheric bore event observed with an all-sky airglow imager at Tirunelveli (8.7°N). J. Geophys. Res. 114, D08114. https://doi.org/10.1029/2008JD010602.

Patra, A.K., Taori, A., Chaitanya, P.P., Sripathi, S., 2013. Direct detection of wavelike spatial structure at the bottom of the F region and its role on the formation of equatorial plasma bubble. J. Geophys. Res. Space Phys. 118 (3), 1196–1202. https://doi.org/10.1002/jgra.50148.

Paulino, I., Takahashi, H., Medeiros, A.F., Wrasse, C.M., Buriti, R.A., Sobral, J.H.A., Gobbi, D., 2011. Mesospheric gravity waves and ionospheric plasma bubbles observed during the COPEX campaign. J. Atmos. Sol. Terr. Phys. 73, 1575–1580. https://doi.org/10.1016/j.jastp.2010.12.004.

Prakash, S., Pandey, R., 1985. Generation of electric field due to gravity wave winds and their transmission to other ionospheric regions. J. Atmos. Terr. Phys. 47, 363–374. https://doi.org/10.1016/0021-9169(85)90016-9.

Rishbeth, H., 1971a. The *F*-layer dynamo. Planet. Space Sci. 19 (2), 263–267. https://doi.org/10.1016/0032-0633(71)90205-4.

Rishbeth, H., 1971b. Polarization fields produced by winds in the equatorial *F*-region. Planet. Space Sci. 19 (3), 357–369. https://doi.org/10.1016/0032-0633(71)90098-5.

Sivakandan, M., Paulino, I., Ramkumar, T.K., Taori, A., Patra, A.K., Sripathi, S., Niranjan, K., Bilibio, A.V., 2019. Multi-instrument investigation of troposphere-ionosphere coupling and the role of gravity waves in the formation of equatorial plasma bubble. J. Atmos. Sol. Terr. Phys. 189, 65–79. https://doi.org/10.1016/j.jastp.2019.04.006.

Takahashi, H., Taylor, M.J., Pautet, P.D., Medeiros, A.F., Gobbi, D., Wrasse, C.M., et al., 2009. Simultaneous observation of ionospheric plasma bubbles and mesospheric gravity waves during the SpreadFEx campaign. Ann. Geophys. 27 (4), 1477–1487. https://doi.org/10.5194/angeo-27-1477-2009.

Taori, A., Makela, J.J., Taylor, M., 2010. Mesospheric wave signatures and equatorial plasma bubbles: A case study. J. Geophys. Res. 115, A06302. https://doi.org/10.1029/2009JA015088.

Taori, A., Patra, A.K., Joshi, L.M., 2011. Gravity wave seeding of equatorial plasma bubbles: An investigation with simultaneous F region, E region, and middle atmospheric measurements. J. Geophys. Res. 116 (A5), A05310. https://doi.org/10.1029/2010JA016229.

Taori, A., Kamalakar, V., Joshi, L.M., Sripathi, S., Patra, A.K., 2012. On the linkage between mesospheric gravity waves and occurrence of equatorial plasma bubble observed during the low solar activity. Indian J. Radio Space Phys. 41, 264–270.

Tsunoda, R.T., Bubenik, D.M., Thampi, S.V., Yamamoto, M., 2010. On large-scale wave structure and equatorial spread F without a post-sunset rise of the F layer. Geophys. Res. Lett. 37, L07105. https://doi.org/10.1029/2009GL042357.

Vadas, S.L., 2007. Horizontal and vertical propagation and dissipation ofgravity waves in the thermosphere from lower atmospheric and thermospheric sources. J. Geophys. Res. 112, A06305. https://doi.org/10.1029/2006JA011845.

Varney, R.H., Kelley, M.C., Kudeki, E., 2009. Observations of electric fields associated with internal gravity waves. J. Geophys. Res. 114 (A2), A02304. https://doi.org/10.1029/2008JA013733.

Sripathi, S., Singh, R., Banola, S., Sreekumar, S., Emperumal, K., & Selvaraj, C. (2016). Characteristics of the equatorial plasma drifts as obtained by using Canadian Doppler ionosonde over southern tip of India. Journal of Geophysical Research: Space Physics, 121, 8103–8120.https://doi.org/10.1002/2016ja023088